ACS APPLIED MATERIALS & INTERFACES

Research Article

Cite This: ACS Appl. Mater. Interfaces 2019, 11, 6759−6768

www.acsami.org

Real-Time FO-SPR Monitoring of Solid-Phase DNAzyme Cleavage Activity for Cutting-Edge Biosensing

Bernd Peeters,[†] Devin Daems,[†] Tom Van der Donck,[‡] Filip Delport,[§] and Jeroen Lammertyn*[,†]

[†]Department of Biosystems, Biosensors Group, KU Leuven, Willem de Croylaan 42, B-3001 Leuven, Belgium

[‡]Department of Materials Engineering, KU Leuven, Kasteelpark Arenberg 44, B-3001 Leuven, Belgium

[§]FOx Biosystems NV, Veldstraat 120, B-9140 Temse, Belgium

Supporting Information

ABSTRACT: DNA nanotechnology has a great potential in biosensor design including nanostructuring of the biosensor surface through DNA origami, target recognition by means of aptamers, and DNA-based signal amplification strategies. In this paper, we use DNA nanotechnology to describe for the first time the concept of real-time solid-phase monitoring of DNAzyme cleavage activity for the detection of specific single-stranded DNA (ssDNA) with a fiber optic surface plasmon resonance (FO-SPR) biosensor. Hereto, we first developed a robust ligation strategy for the functionalization of the FO-SPR biosensing surface with ssDNA-tethered gold nanoparticles, serving as the substrate for the DNAzyme. Next, we established a relation between the SPR signal change, due to the cleavage activity of the 10−23 DNAzyme, and the concentration of the DNAzyme, showing faster cleavage kinetics for higher DNAzyme concentrations. Finally, we implemented this generic concept for biosensing of ssDNA target in solution. Hereto, we designed a DNAzyme−inhibitor complex, consisting of an internal loop structure complementary to the ssDNA target, that releases active DNAzyme molecules in a controlled way as a function of the target concentration. We demonstrated reproducible target detection with a theoretical limit of detection of 1.4 nM, proving that the presented ligation strategy is key to a universal DNAzyme-based FO-SPR biosensing concept with promising applications in the medical and agrofood sector.

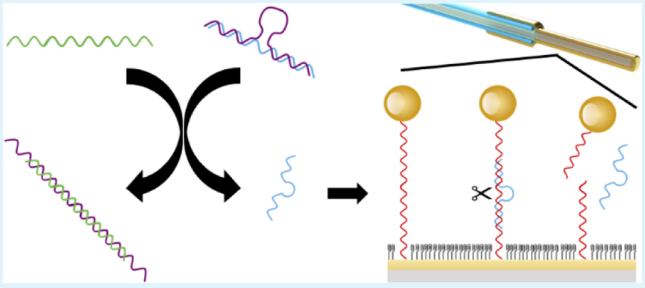

KEYWORDS: *FO-SPR, ligation, gold nanoparticles, DNAzyme, ssDNA detection, biosensor*

1. INTRODUCTION

About 3 decades ago, nucleic acid research revealed that RNA and DNA functionality by far exceeds simple storage and transfer of genetic information. With the development of functional nucleic acids (NAs) through in vitro synthesis and selection by systematic evolution of ligands by exponential enrichment,[1−3] DNA nanotechnology has become a research field on its own with many applications in different areas.[4] In biosensing, DNA molecules and structures are mainly being used for nanostructuring of sensor surfaces,[5] target recognition,[6] and signal amplification.[7] The advantages of using functional NAs are based on their in vitro and cost-effective synthesis, various conjugation options, increased stability, and reduced susceptibility to nonspecific adsorption, compared to their protein alternatives such as antibodies and enzymes.[6] Whereas aptamers show high affinity for specific target molecules, NA enzymes such as DNAzymes are of great interest in isothermal signal generation and amplification.[7,8] Among the broad variety of DNAzymes, peroxidase-mimicking and RNA-cleaving DNAzymes are commonly used for the detection of proteins and NAs.[9] Peroxidase-mimicking DNAzymes are characterized by a G-quadruplex that binds hemin and catalyzes the oxidation of substrates[10] such as H_2O_2, tetramethylbenzidine, and luminol, enabling electrochemical,[11] colorimetric,[12,13] chemiluminescent,[14,15] and surface plasmon resonance (SPR)[16,17] read out. RNA-cleaving DNAzymes are characterized by a small catalytic core accompanied by two binding arms, showing stable activity in the presence of their metal ion cofactors.[18,19] Two well-known RNA-cleaving DNAzymes are the 10−23 and the 8−17 DNAzymes,[19] characterized by high catalytic efficiencies and design flexibility. Their enzymatic activity is only determined by the catalytic core, enabling substantial freedom in redesigning the binding arms for any RNA or DNA/RNA chimeric substrates of interest.

Commonly, RNA-cleaving DNAzyme substrates are labeled with a fluorophore and quencher, resulting in a solution-based, direct fluorescent read-out upon substrate cleavage.[8,9] First applications restricted themselves to the detection of metal targets, based on the intrinsic DNAzyme characteristic of needing a metal cofactor for activity.[8] Extension of the nonmetallic target repertoire is more challenging, yet possible

Received: October 26, 2018
Accepted: January 25, 2019
Published: January 25, 2019

DOI: 10.1021/acsami.8b18756
ACS Appl. Mater. Interfaces 2019, 11, 6759−6768

using strategies in which the DNAzyme is blocked[20] in the absence of a target or by splitting the catalytic core to form so-called binary deoxyribozymes[21] or MNAzymes.[22−24] Several efforts have been reported to improve the background signal of these fluorescent substrates with different configurations of organic quenchers.[25−29] However, another promising alternative is to move completely away from fluorescence and use the (non-) intact substrate or other secondary strands for the indirect signal generation with different read-out systems. Electrochemical,[30,31] colorimetric,[32] and few SPR[33,34] strategies have been described that keep the NAzyme activity in solution but still require an additional hybridization or labeling step for indirect signal generation.

A different approach is to immobilize the DNAzymes and/or their substrates to a solid surface, confining the DNAzyme activity at this solid surface. Based on various conjugation possibilities of NAs, different nanomaterials[35,36] and planar surfaces[37] can be functionalized and act as fluorescence quenchers. In addition, surface immobilization allows washing steps, minimizing potential background signals. Besides fluorescence, researchers have been developing DNAzyme-based solid-phase systems in combination with different labels such as nanoparticles (NPs)[38] and electrochemically active components,[16,39] avoiding complex and dual labeling of substrates with fluorophores and quenchers. So far, sensing applications of surface-immobilized RNA-cleaving DNAzymes or their substrates are mainly restricted to the detection of their metal cofactors.[40] In contrast, direct solid-phase monitoring of NAzyme activity on the surface has not been reported for the detection of NAs or proteins.

SPR is a solid-phase technology and known as the gold standard for molecular interaction analysis. The technology uses an evanescent wave at the sensor's interface to measure changes in refractive index (RI) caused by specific interaction between surface-immobilized receptors and target molecules.[41,42] Starting from complex and bulky prism-based microfluidic systems, SPR technology has been developed into more user-friendly and cost-effective configurations, such as optical fibers.[43,44] An in-house-developed fiber optic SPR sensor (FO-SPR) was previously reported by our group.[45] FO-SPR can compete in sensitivity and specificity with the prism-based systems due to their compatibility with gold nanoparticles (AuNPs) for signal amplification.[46] However, not only binding of AuNPs labels but also the release of AuNPs from the surface has been used to design sensitive bioassays, such as high-resolution melting assays.[47] In addition, the FO-SPR technology has proven its value in biosensing applications for the detection of DNA, proteins, and small molecules.[48−50] Furthermore, compared to other standard techniques, the FO-SPR platform is capable of real-time monitoring, quantifying kinetic measurements and fast sample analysis.

Based on the limitations of the NAzyme-based fluorescent sensors and restricted biosensing applications of surface immobilized NAzymes and substrates, the primary objective of this work is the development of an innovative, solid-phase biosensing concept sensitive to surface-based catalytic cleavage activity of NAzymes. Instead of secondary hybridization or labeling of NAzyme products on the surface, the research focused on the direct interaction between surface-tethered substrates and NAzymes to create an associated response signal. Direct solid-phase monitoring of NAzyme activity has the advantage to enable integration of the signal transduction into NAzyme cascades amplifying the amount of NAzyme itself,[23,51,52] enabling reduced assay times. These type of NAzyme cascades are of great interest, as increasing the amount of NAzymes intrinsically generates an additional amplification effect due to their catalytic activity. The second aim of this work is to show the potential of the proposed solid-phase sensor concept toward biosensing applications. This way, the interesting advantages of NAzymes DNA nanotechnology such as their specificity, isothermal signal generation, and amplification could be explored to create new NAzyme-based bioassay concepts. Furthermore, in combination with detection strategies only redesigning the initial step of the amplification cascade but keeping the NAzyme binding arms and substrate strand constant, a universal solid-phase sensor could be developed for different targets such as proteins and NAs.

To do so, we present for the first time the development of a AuNP-labeled FO-SPR sensor and a generic DNAzyme-based bioassay concept for single-stranded DNA (ssDNA) detection. The FO-SPR platform was selected based on several features such as its AuNP compatibility, dip probe format, and real-time analysis capacity of molecular binding events. First, a ligation strategy was designed to prefunctionalize and optimize the FO-SPR sensors with AuNP-labeled DNAzyme substrates. Second, DNAzyme detection was established by monitoring the corresponding FO-SPR shifts for different DNAzyme concentrations in real time. As a proof of concept, a third section focused on the detection of a ssDNA target strand by temporary blocking the DNAzyme with an inhibitor strand, containing an internal loop for target recognition. Target detection was established, revealing that in combination with its real-time aspect, user-friendliness, and fast response time, FO-SPR technology holds great potential in the study of surface-based NAzyme cleavage activity and the development of innovative NAzyme-based bioassay concepts for NA detection.

2. EXPERIMENTAL SECTION

2.1. Materials and Reagents. All DNA sequences were synthesized and purified by Integrated DNA Technologies (IDT, Leuven, Belgium). Full sequence information is provided in Table S1 of the Supporting Information. Trizma base, sodium dodecyl sulfate (SDS), magnesium chloride, and DNA/RNAse-free water were purchased from The Merck group-Sigma-Aldrich (Bornem, Belgium). Potassium dihydrogen phosphate and sodium chloride were obtained from The Thermo Fisher Scientific group-Fisher Scientific (Merelbeke, Belgium), and dipotassium hydrogen phosphate and 1,4-dithiothreitol (DTT) from AppliChem GmbH (Darmstadt, Germany). Ethylenediaminetetraacetic acid (EDTA) was purchased from Acros Organics (Geel, Belgium), sodium hydroxide from Chemlab (Zedelgem, Belgium), and ethanol absolute from VWR Chemicals (Haasrode, Belgium). Both Illustra NAP-5 columns and Immobiline DryStrip Cover Fluid were obtained from GE Healthcare Life Sciences (Diegem, Belgium). AuNPs (Ø 20 nm) were provided by BBI Solutions (Cardiff, U.K.) and poly(ethylene glycol) (PEG)-molecules ($C_{27}H_{55}NO_9S$), used as a backfilling molecule, by Polypure AS (Oslo, Norway). The Ampligase Thermostable DNA Ligase (5 U/μL) with accompanying 10× reaction buffer was purchased from Epicentre (Madison). Nondenaturing TBE gels (10%) and 5× TBE buffer were obtained from The Thermo Fisher Scientific group—Invitrogen (Merelbeke, Belgium) and 6× Orange DNA Loading Dye from The Thermo Fisher Scientific group—Thermo Scientific (Merelbeke, Belgium).

Sensor preparation and reaction buffers were as follows: PB buffer (180 mM phosphate, pH 8), PB−SDS buffer (10 mM phosphate, 0.01% (w/v) SDS, pH 8.0), TE buffer (10 mM Tris, 1 mM EDTA, pH 8), Tris−SDS buffer (20 mM Tris buffer, 0.01% (w/v) SDS, pH

DOI: 10.1021/acsami.8b18756
ACS Appl. Mater. Interfaces 2019, 11, 6759−6768

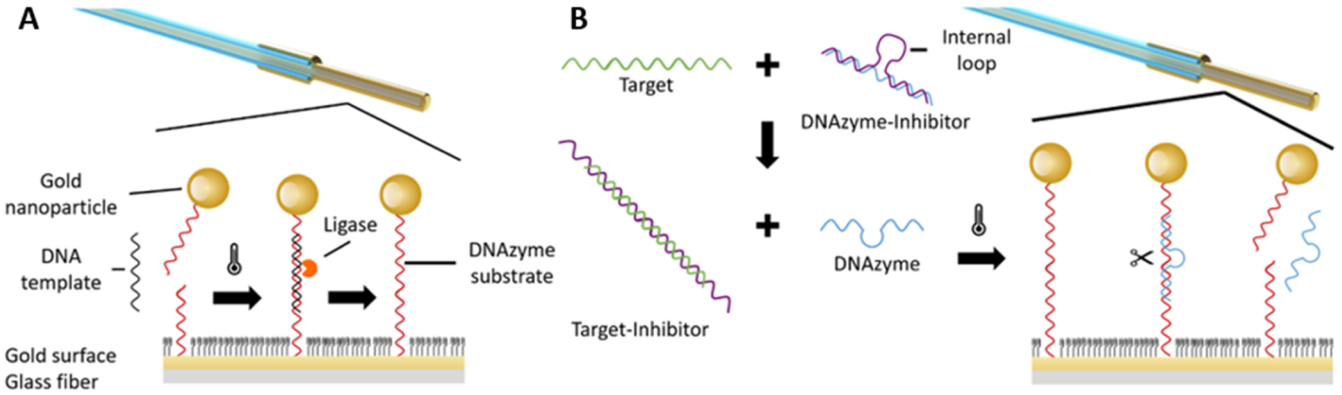

Figure 1. Illustration of (A) the ligation strategy and (B) the DNAzyme-based target detection.

8.3), and DNAzyme reaction buffer (20 mM $MgCl_2$, 50 mM Tris, 150 mM NaCl, pH 9.4).

2.2. FO-SPR Sensor Fabrication and Gold Surface Functionalization. An overview of the FO-SPR experimental setup is presented in the Supporting Information (Figure S1). Production of the FO-SPR sensors was based on the design described by Lu et al.[49] Briefly, an optical fiber (Thorlabs, Newton) (Ø 400 μm) was cut to a final length of 4.3 cm. Both endings were stripped and cleaned to remove the jacket and cladding, respectively. The FO-SPR sensor was coated with a 50 nm gold layer, after which the FO-SPR sensor was ready for functionalization. The gold surfaces were functionalized based on the work of Hurst et al. and Daems et al.[48,53] Both the FO-SPR sensors and the AuNPs were incubated with 1 μM thiolated DNA strands (Table S1), reduced in 0.05 M DTT in PB buffer prior to use. After an overnight incubation, the FO-SPR sensors and AuNPs were washed with Tris−SDS (dipped 5× in 2 mL) and PB−SDS (3× centrifuging at 16 200*g* for 15 min and resuspended in a final volume of 1 mL). Next, backfilling of the FO-SPR sensors and AuNPs was done with 50 μM PEG-molecules for 1 h. The FO-SPR sensors were then washed with and stored in Tris−SDS at 4 °C until further use. The AuNPs were washed two times with PB−SDS and finally resuspended in DNA/RNAse-free water to a final concentration of 4.65 nM by measuring the maximal optical density at 530 nm with a microplate reader SpectraMax M2/M2e (Molecular devices, San Jose).

2.3. AuNP Ligation to the FO-SPR Sensor Surface. A AuNP-labeled DNAzyme substrate coupled to the FO-SPR sensors was created by means of ligation. A ligation reaction mix was prepared containing 1× Ampligase buffer, 0, 10, 100, or 1000 nM of ligation template, Ampligase (0.05 U/μL), and 2.32 nM functionalized AuNPs in a final volume of 100 μL. Prior to ligation, a baseline signal was established for 5 min in 20 mM Tris (pH 8.3), followed by incubation of the FO-SPR sensors in the ligation mixture for 20 min. Next, the FO-SPR sensors were washed for 4 min in 20 mM Tris (pH 8.3), 2 times for 30 s in 10 mM NaOH, and afterward a second baseline was recorded in Tris buffer. All reaction vials were heated simultaneously to 50, 55, or 60 °C and covered with 50 μL mineral oil (to avoid evaporation). The FO-SPR signals were monitored in real-time on an in-house-developed FO-SPR system described by Lu et al.[49] Finally, the AuNP-labeled FO-SPR sensors were stored in Tris−SDS at 4 °C until further use in the DNAzyme-based experiments.

2.4. Real-Time FO-SPR Monitoring of DNAzyme Activity. DNAzyme reaction mixtures contained DNAzyme reaction buffer and 0, 0.1, 1, 3.125, 6.250, 10, 12.5, 25, 50, or 100 nM DNAzyme in a final volume of 100 μL. A first baseline was established in DNAzyme reaction buffer for 7 min, followed by incubation of the FO-SPR sensors in one of the DNAzyme reaction mixtures for 30 min. The catalytic reaction was stopped by washing two times for 30 s with 10 mM NaOH, 1 time for 30 s with TE buffer, and afterward a second baseline was recorded in the DNAzyme reaction buffer. All reaction vials were heated simultaneously at 55 °C and covered with mineral oil.

2.5. DNAzyme Blocking with Inhibitor Strand. Different concentrations of 100, 140, or 180 nM inhibitor strand were mixed in DNAzyme reaction buffer with a fixed DNAzyme concentration of 100 nM. After 30 s heating at 95 °C and incubation at 55 °C for 30 min, the inhibitor−DNAzyme complex was cooled and stored at 4 °C. DNAzyme inhibition experiments were performed identically to the DNAzyme activity experiments, but instead of different DNAzyme concentrations, the FO-SPR sensors were incubated with a four-time dilution of the different inhibitor−DNAzyme mixtures in DNAzyme buffer.

2.6. DNAzyme-Based Target Detection. Target concentrations of 0, 10, 12.5, 15, 20, 25, or 30 nM and 30 nM of nonmatching ssDNA (Table S1) were incubated at 55 °C for 20 min in DNAzyme reaction buffer together with a 1.4:1 ratio of inhibitor−DNAzyme complex prepared as aforementioned prior to starting the DNAzyme activity read out. Read out of the DNAzyme activity was performed as described earlier, except for the first baseline. This baseline was prolonged to 10 min, making a total of 30 min incubation of the ssDNA target with the DNAzyme−inhibitor complex before starting the read out.

2.7. Scanning Electron Microscopy (SEM) Images and Data Analysis. High-resolution scanning electron microscopy (SEM) images were made with a FEI Nova Nanosem 450 (The Thermo Fisher Scientific group—FEI, Hillsboro). Visualization of the 20 nm AuNPs was established with a backscatter detector (concentric backscatter detector) using an acceleration voltage of 4.5 kV in the column and a magnification of 100 000. Applying a bias of 4 kV on the sample stage enabled beam deceleration and resulted in a landing energy of 500 V. To obtain a stable imaging, drift-corrected frame integration was used. The difference in contrast of the images could be explained by small differences in the sample preparation and different position of the image on the FO-SPR sensor surface. Quantification of the AuNPs was done by using ImageJ 1.48 v (National Institutes of Health, Bethesda),[54] a Java-based image-processing program. All SEM images having a surface area of 7.5 μm^2 were sharpened if needed and after setting the proper noise tolerance, the AuNPs could be counted using the "Find Maxima" tool in ImageJ. For every condition, the AuNP density was determined for three images at different locations on the same fiber.

FO-SPR data were recorded with LabView (National Instruments, Austin) and further processed using Matlab 2015b (The MathWorks Inc., Natick). All FO-SPR signals start with an initial baseline measurement in simple buffer conditions. By determining the average wavelength value across this baseline step and subtracting it from the complete FO-SPR signal, the starting FO-SPR wavelength for every sensorgram was normalized to 0 nm. Based on the different steps within both the ligation an DNAzyme activity sensorgrams, different parameters were defined to enable statistical analysis with JMP 13 (SAS Institute Inc., Cary): (i) ligation shift, (ii) DNAzyme shift, (iii) ligation efficiency, (iv) DNAzyme efficiency, and (v) half time value. Significant differences were analyzed by performing one-way ANOVA followed by Tukey multiple comparison with an α-level of 0.05.

DOI: 10.1021/acsami.8b18756
ACS Appl. Mater. Interfaces 2019, 11, 6759−6768

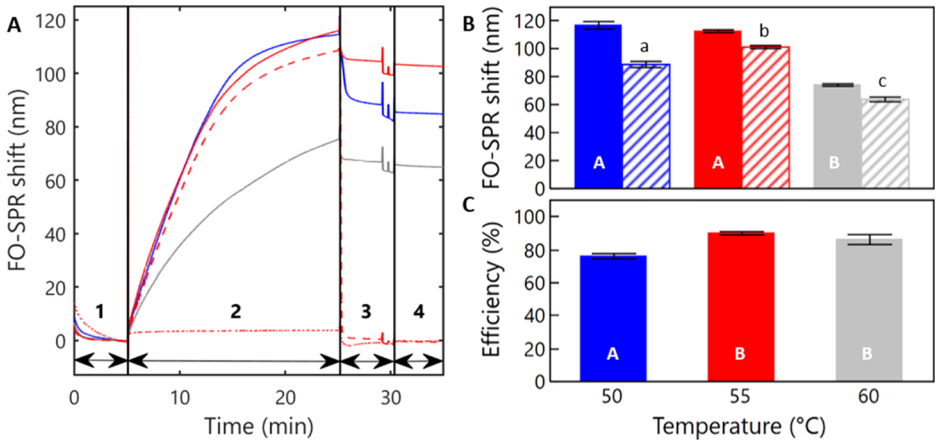

Figure 2. Ligation temperature screening. (A) Real-time FO-SPR shifts for ligation at 50 °C (blue), 55 °C (red), and 60 °C (gray). Controls containing no ligase (dashed line) or no template (dotted line) were included to evaluate nonspecific adsorption at 55 °C. Every measurement consists of four steps: (1) first baseline in buffer, (2) hybridization and ligation, (3) washing, and (4) second baseline in buffer. (B) FO-SPR shifts before washing (filled bars) and final ligation shifts after washing (shaded bars) and (C) ligation efficiency. Error bars represent one standard deviation (n = 4). Upper- or lower-case letters group the factor levels between which Tukey multiple comparison was applied. Different letters indicate significant differences ($P < 0.05$).

Calibration curves were linearly fitted by $y = ax + b$, with y as the logarithmic half-life values, x as the logarithmic concentration, a as the slope, and b as the intercept. The limit of detection (LOD) was based on the linear regression and calculated as LOD = $3 \times \sigma/S$, with σ as the standard deviation of the response estimated by the root mean squared error (RMSE) and S as the slope of the calibration curve.[55]

3. RESULTS AND DISCUSSION

3.1. Concept of DNAzyme-Based FO-SPR Biosensing. The ligation strategy to functionalize FO-SPR sensors with AuNP-labeled substrates is depicted in Figure 1A. Three DNA oligos are used to perform the ligation: (i) a 5′-thiolated FO-SPR oligo immobilized on the FO-SPR sensor surface, (ii) a 3′-thiolated AuNP-oligo immobilized on the AuNP surface, and (iii) a ligation template partially complementary to both FO-SPR and AuNP-oligo. Upon hybridization of the FO-SPR and AuNP-oligo with the ligation template, the ligase recognizes the nick in the double DNA strand and links the 5′-phosporylated AuNP-oligo with the FO-SPR oligo by a NAD-dependent ligation. As a result, AuNP-labeled DNAzyme substrates are formed. AuNP labels are well-known to significantly amplify the FO-SPR response signals[56] and are introduced here to enable real-time direct monitoring of the DNAzyme cleavage activity. Furthermore, the FO-SPR and AuNP-oligos are designed in such a way that both DNA oligos contain part of the DNAzyme substrate each, eliminating DNAzyme cleavage of unlabeled substrates. Figure 1B illustrates the DNAzyme-based target detection using the designed FO-SPR sensor. The system includes three additional DNA oligos: (i) a synthetic, specific DNA target, (ii) a DNAzyme, and (iii) a ssDNA inhibitor. The inhibitor is designed to block the DNAzyme by partial hybridization. It contains a loop of 22 nucleotides, which can be adapted to any target without changing the DNAzyme sequence. In the presence of the target, the inhibitor preferentially binds the DNA target of interest due to higher complementarity and therefore resulting in a lower ΔG compared to the interaction with the DNAzyme. This way, the DNAzyme is activated and can start cleaving the AuNP-labeled substrate on the FO-SPR sensor.

To realize the proposed DNAzyme-based FO-SPR sensor, the first set of experiments is devoted to finding an optimal ligation temperature and template concentration for AuNP labeling of the FO-SPR oligos. Second, the activity of different DNAzyme concentrations is characterized and a calibration curve is established on the AuNP-labeled FO-SPR sensor. In a third set of experiments, blocking of the DNAzyme is evaluated for different inhibitor−DNAzyme ratios. Finally, different synthetic DNA target concentrations are detected and a calibration curve is established.

3.2. Screening and Optimization of Robust Ligation Strategy. The NAzyme in this work is characterized by a cleave-and-release process, requiring labeled substrates to monitor the surface catalytic activity. Therefore, a ligation strategy, having important advantages such as (i) the covalent linkage of AuNP labels to the DNAzyme substrate, stabilizing and creating a robust sensor surface, and (ii) the elimination of nonlabeled DNAzyme substrates, was used. Cleavable substrates are only formed where ligation has taken place and minimizes the occurrence of DNAzyme cleavage without signal generation. The AuNP labeling of the immobilized FO-SPR oligos on the sensor surface depends on the ligation template concentration, the functionalized AuNP concentration, the amount of ligase, the incubation temperature and time. Both the ligation temperature and template concentration were studied in more detail, whereas other parameters were fixed based on previous work of Knez et al.[47,57] and the Ampligase product specifications.

While changing and studying the parameter of interest, the FO-SPR shift was monitored in real-time and consists of four different steps as illustrated in Figure 2A. Step 1 represents a first stabilization step, which enables the FO-SPR sensor to reach its baseline level. Initial signal drift is caused by a change in RI going from air to buffer and the increasing temperature, as the FO-SPR sensor is temperature sensitive. In step 2, binding of the AuNPs to the FO-SPR sensor surface through hybridization between the ligation template, FO-SPR, and AuNP-oligos causes the FO-SPR shift to increase. The nick in every hybridization complex, if recognized by the ligase, gets covalently coupled to form a AuNP-labeled DNAzyme substrate (Figure 1A). In this step, also the nonligated

DOI: 10.1021/acsami.8b18756
ACS Appl. Mater. Interfaces 2019, 11, 6759−6768

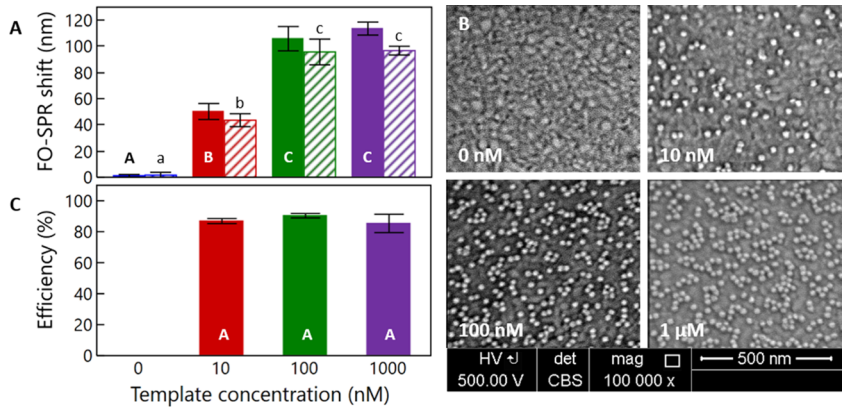

Figure 3. Screening of the ligation template concentration. (A) FO-SPR shifts before washing (filled bars) and final ligation shifts (shaded bars). (B) SEM images of four different FO-SPR sensors after ligation with 0, 10, 100, and 1000 nM ligation template. (C) Ligation efficiency. Error bars represent one standard deviation (n = 4). Upper- or lower-case letters group the factor levels between which Tukey multiple comparison was applied. Different letters indicate significant differences (P < 0.05).

hybridization complexes contribute to the corresponding FO-SPR shift. Step 3 represents a washing step in Tris buffer and two times in NaOH, clearly distinguishable by short RI changes in air when switching reaction vials. During this step, all hybridization complexes are dehybridized, removing all ligation templates and nonligated AuNP labels to make the AuNP-labeled DNAzyme substrates available and avoid any nonspecific release of AuNPs during target detection. Finally, step 4 corresponds to a second stabilization step, which enables the FO-SPR sensor to reach a new baseline level in conditions identical to those of step 1.

Optimal reaction conditions were defined as those resulting in a large FO-SPR shift at the end of step 4. This depends on the hybridization with the ligation template and actual ligation, both taking place in the same reaction vial in step 2. Therefore, the process is strongly dictated by a proper reaction temperature for both hybridization complex formation and ligase activity. The ligation process was first evaluated for three different temperatures while keeping the ligation template concentration constant. As can be seen in step 2, the FO-SPR shifts increase significantly for all temperatures, except for the control experiment evaluating the FO-SPR shift in the absence of ligation template (Figure 2A). Moreover, the exact FO-SPR shifts, determined as the difference between the start- and endpoints of step 2, are similar for 50 and 55 °C but lower for 60 °C (Figure 2B). This depends on the sequence complementarity and melting temperature (T_m) of the formed hybridization complex, being 65.1 ± 0.3 °C (Figure S2). The decrease at 60 °C is explained by the fact that the reaction conditions approach the T_m of the hybridization complex. For similar FO-SPR shifts at 50 and 55 °C, both well below the T_m, it is hypothesized that the change in hybridization equilibrium by the temperature difference of 5 °C is not significant to cause any change in FO-SPR shift. Furthermore, final ligation shifts were determined as the absolute difference between both baselines (steps 1 and 4) after washing (step 3) because hybridization complexes for which no ligation took place only release their noncovalent AuNP labels in step 3. This causes the FO-SPR shifts to decrease again for all temperatures in step 3. As the ligase's activity increases with temperature and has an optimum at 68−72 °C (see product specifications), an increasing ligation shift could be expected. As can be seen, the ligation shifts were found to indeed first increase significantly with temperature and decrease again for 60 °C (this is because of the lower FO-SPR shift at 60 °C in step 2, as explained earlier).

In addition to a large ligation shift, an optimal ligase activity is desired, meaning that all hybridized AuNPs are also ligated to the FO-SPR sensor surface. Ligation efficiencies were also determined as a function of temperature and defined as the ratio of the FO-SPR shift before the wash step and the final ligation shift (Figure 2B,C). Initially, the ligation efficiencies increased significantly, reaching a value of 90.0 ± 1.0% at 55 °C, which did not improve further. Based on the maximal ligation shift of 101.5 ± 2.1 nm and the ligation efficiency of 90.0 ± 1.0%, 55 °C was regarded as the optimal temperature and selected for all further experiments. Compared to the typical range of FO-SPR shifts around 10 nm previously reported,[45,49,50] the range of the obtained FO-SPR shifts is more than 10-fold higher. This can be explained by using relatively short DNA oligos, a higher AuNP concentration, and the specific choice of incubation time and reaction temperature to improve and maximize the FO-SPR parameters such as the FO-SPR shift, the dynamic range, and the LOD.

Furthermore, the screening of the ligation template concentration is visualized in Figure 3. The ligation shifts and ligation efficiencies were monitored in real time (data not shown) and determined for 0, 10, 100, and 1000 nM ligation template. The ligation shift (Figure 3A) for 10 nM ligation template was significantly lower compared to the shift at higher ligation template concentrations. Further increase in the ligation template concentration enabled more AuNPs to bind the FO-SPR sensor and eventually a saturation level on the FO-SPR sensor was reached for template concentrations ≥100 nM. This saturation level is determined both by the geometry and steric interactions of the AuNPs under specified reaction conditions. In addition, the ligation of AuNPs to the FO-SPR sensor surface was evaluated with high-resolution SEM images. Figure 3B shows part of the SEM images made for every ligation condition using different ligation template concentrations (full images in Figure S3). In case of 0 nM ligation template, aspecific binding to the FO-SPR sensor surface caused few AuNPs to emerge, resulting in a AuNP density of 5 ± 6 particles/μm^2 by counting the AuNPs in the SEM images. Furthermore, the SEM image shows the gold islands of the sputtered thin film.[58] By increasing the ligation template concentration, an increasing amount of AuNPs was ligated to the FO-SPR sensor surface: the AuNP densities were 244 ±

DOI: 10.1021/acsami.8b18756
ACS Appl. Mater. Interfaces 2019, 11, 6759−6768

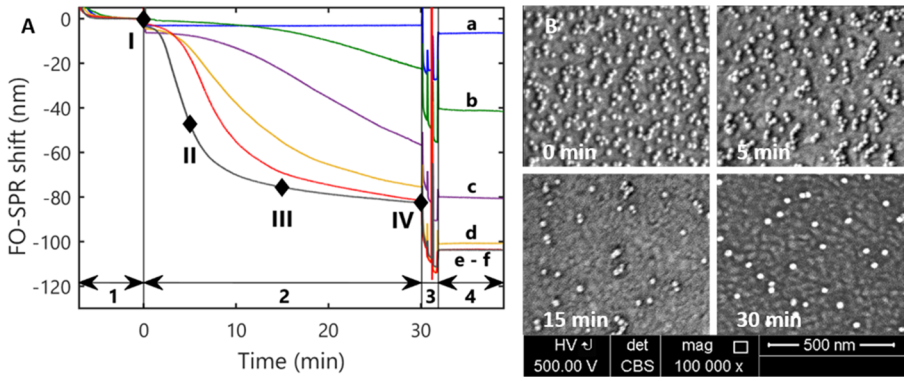

Figure 4. DNAzyme response. (A) Real-time FO-SPR shifts for (a) 0 nM, (b) 3.125 nM, (c) 6.25 nM, (d) 12.5 nM, (e) 25 nM, and (f) 50 nM DNAzyme. Every measurement consisted of four steps: (1) first baseline, (2) DNAzyme incubation, (3) washing, and (4) second baseline and (B) represents the SEM images taken after (I) 0 min, (II) 5 min, (III) 15 min, and (IV) 30 min of incubation with 25 nM DNAzyme.

31, 666 ± 56, and 678 ± 95 particles/μm^2 for 10, 100, and 1000 nM ligation template, respectively. A saturation was obtained for 100 nM ligation template (Figure S4). Figure 3C depicts that the ligation efficiencies do not significantly depend on the template concentration. Based on the saturation of the ligation shifts for template concentrations ≥100 nM, the 100 nM template concentration with a ligation efficiency of 90.3 ± 1.4% was selected and used together with the optimal temperature of 55 °C in all further experiments.

3.3. Characterization of DNAzyme Activity with FO-SPR. On the basis of the AuNP-labeled FO-SPR sensors produced under optimal ligation conditions defined in previous section, here the DNAzyme cleavage activity is studied. The 10−23 DNAzyme was preferred, based on several of its characteristics as mentioned in the introduction section.[18,19] Creating a FO-SPR sensor design sensitive to surface cleavage activity of NAzymes will make the FO-SPR platform more accessible to the increasing popularity and progress in the field of DNA nanotechnology. Interesting features of the NAzyme technology are (i) their intrinsic capacity of signal amplification and (ii) their superior in vitro synthesis, cost-efficiency, and stability compared to protein enzymes.

Figure 4A illustrates the corresponding DNAzyme activity sensorgrams with four steps similar to the ligation strategy. Step 1 represents the first stabilization step to reach a baseline level as discussed previously. In step 2, the substrate cleavage and release of AuNPs were monitored in real time. Reaction kinetics were studied by determining the half-life value of the FO-SPR sensor response. Step 3 represents a washing step, again clearly distinguishable by the short RI changes in air when switching reaction vials. Finally, step 4 corresponds to a second stabilization step, which enabled the quantification of the corresponding FO-SPR shift. Moreover, in combination with the ligation shifts (see previous section), the DNAzyme efficiency was described.

FO-SPR sensors with AuNPs were incubated with DNAzyme concentrations between 0 and 100 nM. SEM images were made of four different FO-SPR sensors after 0, 5, 15, and 30 min incubation with 25 nM DNAzyme (Figure 4B). The SEM images confirm the release of AuNPs by incubation with the DNAzyme over time. The starting AuNP density was 607 ± 28 particles/μm^2, which decreased to 432 ± 26 particles/μm^2 after 5 min, 87 ± 4 particles/μm^2 after 15 min, and 81 ± 1 particles/μm^2 after 30 min (full images in Figure S6). For the negative (NC) control, the AuNP density remained at 571 ± 11 particles/μm^2, illustrating the specificity of the DNAzyme (Figure S5). DNAzyme shifts were defined as the difference between both baselines and DNAzyme efficiencies as the ratio of DNAzyme and ligation shifts (Figure S7). The ligation shift gives the maximal shift that can be expected after incubation with the DNAzyme. Both parameters showed an increasing, logarithmic trend with the DNAzyme concentration up to 12.5 nM DNAzyme, after which the DNAzyme shift saturated, giving a dynamic range of 1 decade. However, introducing the concept of the half-life values determined in step 2 (except for 0 nM DNAzyme, Figure S8) improved the dynamic range up to 100 nM DNAzyme and could make both baselines unnecessary. In Figure 5, a

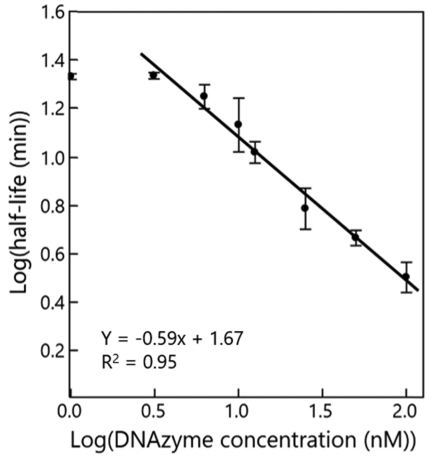

Figure 5. DNAzyme calibration curve. A linear calibration curve was established by log−log transformation of the half-life and DNAzyme concentration. Error bars represent one standard deviation (n = 3).

logarithmic transformation of the exponential part is plotted in the function of the logarithmic DNAzyme concentrations and a linear calibration curve was obtained (R^2 of 0.95) with a RMSE of 0.07. The lowest detectable DNAzyme concentration was 3.125 nM and the theoretical LOD based on the linear regression was 2.3 nM.

3.4. Screening of Inhibitor Concentration for DNAzyme Blocking. To retain a controlled catalytic activity, DNAzyme blocking was established through partial DNA hybridization. The inhibitor strand was designed to be complementary to the DNAzyme's binding arms and part of

DOI: 10.1021/acsami.8b18756
ACS Appl. Mater. Interfaces 2019, 11, 6759−6768

the catalytic core, except for four nucleotides (Figure S9). In addition, one of the blocking regions lacked complementarity with the outer nucleotide of the binding arm and the other blocking region contained a G−T wobble structure.[24] This way, the inhibitor strand with an internal loop was calculated to have a T_m that enables hybridization to the DNAzyme under DNAzyme reaction conditions and dehybridization only by a specific trigger (The DINAmelt Web Server[59,60]). Formation of the duplex between DNAzyme and inhibitor strand was confirmed qualitatively with gel electrophoresis prior to the FO-SPR experiments (Figure S10).

The degree of DNAzyme blocking is steered by the concentration ratio between the inhibitor strand and the DNAzyme. Moreover, there is a trade-off between the background signal and the sensitivity of the assay. To avoid significant background signal, an excess of inhibitor strand is required, whereas to obtain the lowest LOD, the inhibitor strand and the DNAzyme should be present in equimolar ratio. In the final biosensing concept, it is only the DNAzyme-bound fraction of the inhibitor that can trigger signal generation after interaction with the target of interest. Figure S10 illustrates this excess, which becomes visual from the 1.4:1 ratio onward in case of the gel electrophoresis. To minimize the inhibitor excess and still reach a maximal DNAzyme shift, 25 nM DNAzyme was chosen as the concentration to study the FO-SPR shifts in the function of different DNAzyme−inhibitor ratios. Figure 6 presents the FO-SPR shifts obtained for a 1:1, 1.4:1, and 1.8:1 ratio of inhibitor strands and DNAzyme. In comparison with the positive control (PC), not containing any inhibitor, the presence of the inhibitor strand in a 1:1 ratio reduced the FO-SPR shift by more than 50%. Further increase of the inhibitor−DNAzyme ratio resulted in FO-SPR shifts comparable to the negative control (NC), only containing 200 nM inhibitor strand. Therefore, minimal background and inhibitor excess were realized with a ratio of 1.4:1 inhibitor strand and DNAzyme (used in further experiments).

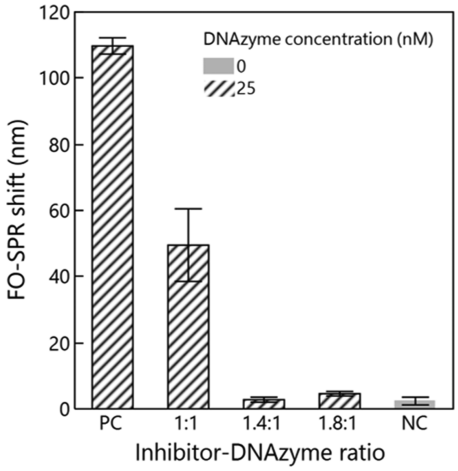

Figure 6. Screening of the inhibitor−DNAzyme ratio for DNAzyme blocking. Positive and negative control (PC and NC) contained only 25 nM DNAzyme and 200 nM inhibitor, respectively. Shaded bars contained 25 nM DNAzyme with increasing amount of inhibitor. Error bars represent one standard deviation (n = 3).

3.5. DNAzyme-Based Detection of a Synthetic DNA Target. Strand displacement[61] was used as the mechanism for target-specific signal generation. By establishing specific target detection, it is shown that the FO-SPR sensor has potential for biosensing applications and that its sensitivity to surface cleavage activity is not restricted to NAzyme monitoring. Hereto, the inhibitor strand with a built-in internal loop (Figure S9) was designed to enable preferential binding to the target in comparison with the DNAzyme. Higher complementarity of the inhibitor strand with the target sequence was provided by the internal loop, whereas the complementary regions were designed to assure blocking of the DNAzyme.

Initially, this target-triggered release of the DNAzyme was first confirmed qualitatively with gel electrophoresis (Figure S11). Next, specific target detection was explored using the same reaction conditions as applied for the real-time DNAzyme activity; however, this time, the DNAzyme was added as a blocked complex with the inhibitor strand as described in previous section. DNAzyme shifts and efficiencies, triggered by different target concentrations and a blank containing a nonmatching ssDNA strand, were determined for all response signals as mentioned in Section 3.3 (Figure S12). FO-SPR shifts increased with target concentration, but no significant FO-SPR shifts were observed in the absence of the target or in the presence of scrambled ssDNA. Based on the half-life values obtained for 0, 10, 12.5, 15, 20, 25, and 30 nM of target DNA, a calibration curve was established. Both the DNAzyme shifts and DNAzyme efficiencies increased with elevated target concentrations. In contrast to the DNAzyme-only experiments, a sigmoidal trend was observed. We hypothesize that the inhibitor excess, needed to assure complete DNAzyme blocking, caused the initial lag in signal generation. Furthermore, the FO-SPR shifts saturated from 15 nM DNA target onward. Therefore, half-life values of the FO-SPR response signals were determined (Figure S13) and a log−log transformation was performed like the DNAzyme-only results (Figure 5). Based on the log−log transformation of the half-life values, the kinetic information within the response signal was used to improve and increase the dynamic range compared to the use of the endpoint DNAzyme shifts. The logarithm of the half-life values was observed to decrease linearly (R^2 = 0.94) with the logarithmic target concentration (Figure 7). An RMSE of 0.08 was obtained and the theoretical LOD was calculated to be 1.4 nM.

On the basis of these results, we demonstrated the potential of a user-friendly, innovative DNAzyme-based FO-SPR

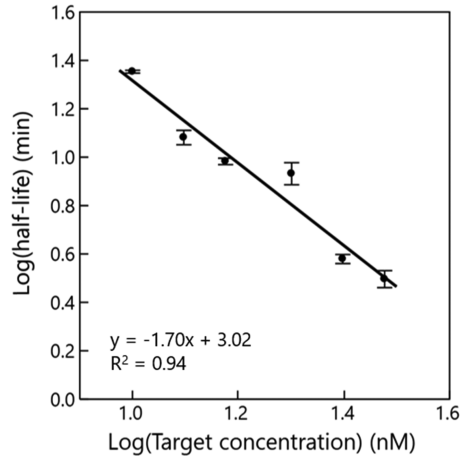

Figure 7. Log−log linear calibration curve of the half-life values and target concentration from 10 to 30 nM. Error bars represent one standard deviation (n = 3).

DOI: 10.1021/acsami.8b18756
ACS Appl. Mater. Interfaces 2019, 11, 6759−6768

biosensor for the specific detection of DNA biomarkers. In comparison to our previous work focusing on the classical AuNP-amplified "sandwich" approach for protein and NA detection, we extended the sensor's applicability to surface catalytic DNA−DNA/RNA interactions with prospects of a potential study tool for these catalytic molecules. To do so and to make a robust sensor design, the classical sandwich approach in combination with ligation was applied for surface functionalization. Furthermore, we showed that the proposed FO-SPR sensor design can be developed toward biosensing applications by illustrating its capacity of ssDNA detection. The LOD was calculated to be 1.4 nM, which is similar to the previously reported 1 nM detection limit of our system for NA detection only using AuNP amplification.[62] Lower pM and sub-pM detection limits have been obtained,[48,57] but require additional amplification of the target strand by polymerase chain reaction or ligase chain reaction, increasing the number of experimental steps and assay time to an hour or several hours depending on the target. By developing a DNAzyme-based FO-SPR sensor design, isothermal and protein-free NAzyme amplification strategies[23] or the use of other RNA-cleaving NAzymes can now be explored to improve specificity and reach pM−fM detection limits. Other SPR sensors using RNA-cleaving NAzymes have already been reported with lower pM[34] and high fM[33] detection limits for NAs and proteins respectively. However, these systems also apply additional indirect amplification strategies such as RNA transcription or catalyzed hairpin assembly with assay times ≥hours and multiple incubation steps. So far, the proposed DNAzyme-based sensor in this work is the first to use FO-SPR, which typically requires smaller sample volume (<100 μL) compared to the prism-based systems. On the other hand, because these prism-based systems mainly detect NAzymes indirectly, their surface can be regenerated, whereas the proposed FO-SPR sensor is for one-time use only. Other optical biosensors using RNA-cleaving NAzymes are those using AuNP aggregation, depending on the intact substrates linking them together. Although cost-effective and user-friendly, most of these systems have been used for the detection of metal ions and few have been reported on biological targets.[32,63]

4. CONCLUSIONS

In this paper, we demonstrated for the first time a robust ligation strategy, linking DNA-functionalized AuNPs covalently to the surface of a FO-SPR sensor. Specific sequence design in combination with ligation enabled both formation and immobilization of AuNP-labeled DNAzyme substrates. Moreover, the ligation strategy eliminated the presence of nonlabeled substrates, minimizing the interference with efficient signal generation. The AuNP surface density was controlled through the selection of the ligation temperature and ligation template concentration. Once the AuNP-labeled DNAzyme substrates were immobilized, real-time detection of surface-based DNAzyme cleavage activity using FO-SPR was reported for the first time and a calibration curve for different DNAzyme concentrations was obtained. Finally, the proposed FO-SPR sensor's potential in developing NAzyme-based biosensing applications was proven. Using partial complementarity and the principle of strand displacement, DNAzymes were temporarily blocked with an inhibitor strand. Preferred complementarity between a ssDNA target and the inhibitor strand enabled specific, DNAzyme-based target detection. By exploiting the half-life values of the FO-SPR response signal, a calibration curve was obtained with a theoretical LOD of 1.4 nM.

In future work, the emphasis will lie on the integration of the designed FO-SPR sensor in NAzyme-based cascades amplifying the NAzyme itself to further improve the current LOD. Another approach is to change the AuNP size, shape, and density to optimize the mass and coupling effect of the particles to improve the sensor's performance. Moreover, the designed bioassay concept displays some interesting flexibility in the choice of DNAzyme substrate and target of interest. Redesigning the ligation template and associated FO-SPR and AuNP-oligo could enable the use of different substrates. On the other hand, it is hypothesized that detection of different targets with the same DNAzyme and substrate used in this work could be obtained by modifying the internal loop of the inhibitor strand. The potential of the designed FO-SPR sensor to be integrated in other DNAzyme-based systems or to be modified toward different targets gives the sensor a universal character. Based on these characteristics, the FO-SPR design should be further adapted toward a real target of interest and compatibility in biological matrices should be validated. In these matrices, challenges such as nonspecific adsorption and potential degradation of DNA components by nucleases or interference with the assay mechanism can be encountered. As the FO-SPR platform is fully automated and able to perform four measurements at the same time, parallel detection of different targets based on one universal FO-SPR sensor would be feasible.

■ ASSOCIATED CONTENT

Supporting Information

The Supporting Information is available free of charge on the ACS Publications website at DOI: 10.1021/acsami.8b18756.

DNA sequences; overview of the FO-SPR setup; melting analysis for T_m determination of ligation template; SEM images and AuNP densities of the ligation; SEM images of the DNAzyme activity; DNAzyme shifts, efficiencies and half-life values for all DNAzyme concentrations; DNAzyme−inhibitor complex structure; polyacrylamide gel electrophoresis analysis of DNAzyme inhibition and target detection; DNAzyme shifts, efficiencies and half-life values for all ssDNA target concentrations (PDF)

■ AUTHOR INFORMATION

Corresponding Author

*E-mail: jeroen.lammertyn@kuleuven.be. Tel: +32 16321459.

ORCID

Bernd Peeters: 0000-0002-9430-0025

Jeroen Lammertyn: 0000-0001-8143-6794

Author Contributions

B.P. designed the experiments, carried out the experiments, and wrote the paper; D.D. designed the experiments, supervised the work, and prepared the manuscript; T.V.d.D. provided technical support for the SEM imaging; F.D. provided suggestions and technical support on the project; J.L. designed the experiments, supervised the work, and prepared the manuscript. All authors discussed the results and commented on the manuscript.

Notes

The authors declare no competing financial interest.

DOI: 10.1021/acsami.8b18756
ACS Appl. Mater. Interfaces 2019, 11, 6759−6768

■ ACKNOWLEDGMENTS

The authors gratefully acknowledge the financial support from KU Leuven and Fund for Scientific Research (FWO-Flanders Postdoctoral Fellow D.D. 12U1618N).

■ REFERENCES

(1) Robertson, D. L.; Joyce, G. F. Selection in Vitro of an RNA Enzyme That Specifically Cleaves Single-Stranded DNA. *Nature* **1990**, *344*, 467−468.
(2) Tuerk, C.; Gold, L. Systematic Evolution of Ligands by Exponential Enrichment: RNA Ligands to Bacteriophage T4 DNA Polymerase. *Science* **1990**, *249*, 505−510.
(3) Ellington, A. D.; Szostak, J. W. In Vitro Selection of RNA Molecules That Bind Specific Ligands. *Nature* **1990**, *346*, 818−822.
(4) Zahid, M.; Kim, B.; Hussain, R.; Amin, R.; Park, S. DNA Nanotechnology: A Future Perspective. *Nanoscale Res. Lett.* **2013**, *8*, 119.
(5) Pei, H.; Zuo, X.; Pan, D.; Shi, J.; Huang, Q.; Fan, C. Scaffolded Biosensors with Designed DNA Nanostructures. *NPG Asia Mater.* **2013**, *5*, No. e51.
(6) Song, K.-M.; Lee, S.; Ban, C. Aptamers and Their Biological Applications. *Sensors* **2012**, *12*, 612−631.
(7) Silverman, S. K. In Vitro Selection, Characterization, and Application of Deoxyribozymes That Cleave RNA. *Nucleic Acids Res.* **2005**, *33*, 6151−6163.
(8) Gong, L.; Zhao, Z.; Lv, Y.-F.; Huan, S.-Y.; Fu, T.; Zhang, X.-B.; Shen, G.-L.; Yu, R.-Q. DNAzyme-Based Biosensors and Nanodevices. *Chem. Commun.* **2015**, *51*, 979−995.
(9) Peng, H.; Newbigging, A. M.; Wang, Z.; Tao, J.; Deng, W.; Le, X. C.; Zhang, H. DNAzyme-Mediated Assays for Amplified Detection of Nucleic Acids and Proteins. *Anal. Chem.* **2018**, *90*, 190−207.
(10) Travascio, P.; Li, Y.; Sen, D. DNA-Enhanced Peroxidase Activity of a DNA Aptamer-Hemin Complex. *Chem. Biol.* **1998**, *5*, 505−517.
(11) Pelossof, G.; Tel-Vered, R.; Elbaz, J.; Willner, I. Amplified Biosensing Using the Horseradish Peroxidase-Mimicking DNAzyme as an Electrocatalyst. *Anal. Chem.* **2010**, *82*, 4396−4402.
(12) Xiao, Y.; Pavlov, V.; Niazov, T.; Dishon, A.; Kotler, M.; Willner, I. Catalytic Beacons for the Detection of DNA and Telomerase Activity. *J. Am. Chem. Soc.* **2004**, *126*, 7430−7431.
(13) Du, Y.; Li, B.; Guo, S.; Zhou, Z.; Zhou, M.; Wang, E.; Dong, S. G-Quadruplex-Based DNAzyme for Colorimetric Detection of Cocaine: Using Magnetic Nanoparticles as the Separation and Amplification Element. *Analyst* **2011**, *136*, 493−497.
(14) Pavlov, V.; Xiao, Y.; Gill, R.; Dishon, A.; Kotler, M.; Willner, I. Amplified Chemiluminescence Surface Detection of DNA and Telomerase Activity Using Catalytic Nucleic Acid Labels. *Anal. Chem.* **2004**, *76*, 2152−2156.
(15) Xia, H.; Li, L.; Yin, Z.; Hou, X.; Zhu, J.-J. Biobar-Coded Gold Nanoparticles and DNAzyme-Based Dual Signal Amplification Strategy for Ultrasensitive Detection of Protein by Electrochemiluminescence. *ACS Appl. Mater. Interfaces* **2015**, *7*, 696−703.
(16) Pelossof, G.; Tel-Vered, R.; Willner, I. Amplified Surface Plasmon Resonance and Electrochemical Detection of Pb 2+ Ions Using the Pb 2+ -Dependent DNAzyme and Hemin/G-Quadruplex as a Label. *Anal. Chem.* **2012**, *84*, 3703−3709.
(17) Li, H.; Chang, J.; Hou, T.; Li, F. HRP-Mimicking DNAzyme-Catalyzed in Situ Generation of Polyaniline To Assist Signal Amplification for Ultrasensitive Surface Plasmon Resonance Biosensing. *Anal. Chem.* **2017**, *89*, 673−680.
(18) Breaker, R. R.; Joyce, G. F. A DNA Enzyme That Cleaves RNA. *Chem. Biol.* **1994**, *1*, 223−229.
(19) Santoro, S. W.; Joyce, G. F. A General Purpose RNA-Cleaving DNA Enzyme. *Proc. Natl. Acad. Sci. U.S.A.* **1997**, *94*, 4262−4266.
(20) Navani, N. K.; Li, Y. Nucleic Acid Aptamers and Enzymes as Sensors. *Curr. Opin. Chem. Biol.* **2006**, *10*, 272−281.
(21) Kolpashchikov, D. M. A Binary Deoxyribozyme for Nucleic Acid Analysis. *ChemBioChem* **2007**, *8*, 2039−2042.
(22) Mokany, E.; Bone, S. M.; Young, P. E.; Doan, T. B.; Todd, A. V. MNAzymes, a Versatile New Class of Nucleic Acid Enzymes That Can Function as Biosensors and Molecular Switches. *J. Am. Chem. Soc.* **2010**, *132*, 1051−1059.
(23) Bone, S. M.; Hasick, N. J.; Lima, N. E.; Erskine, S. M.; Mokany, E.; Todd, A. V. DNA-Only Cascade: A Universal Tool for Signal Amplification, Enhancing the Detection of Target Analytes. *Anal. Chem.* **2014**, *86*, 9106−9113.
(24) Bone, S. M.; Lima, N. E.; Todd, A. V. DNAzyme Switches for Molecular Computation and Signal Amplification. *Biosens. Bioelectron.* **2015**, *70*, 330−337.
(25) Li, J.; Lu, Y. A Highly Sensitive and Selective Catalytic DNA Biosensor for Lead Ions. *J. Am. Chem. Soc.* **2000**, *122*, 10466−10467.
(26) Stojanovic, M. N.; de Prada, P.; Landry, D. W. Catalytic Molecular Beacons. *ChemBioChem* **2001**, *2*, 411−415.
(27) Mei, S. H. J.; Liu, Z.; Brennan, J. D.; Li, Y. An Efficient RNA-Cleaving DNA Enzyme That Synchronizes Catalysis with Fluorescence Signaling. *J. Am. Chem. Soc.* **2003**, *125*, 412−420.
(28) Liu, J.; Lu, Y. Improving Fluorescent DNAzyme Biosensors by Combining Inter- and Intramolecular Quenchers. *Anal. Chem.* **2003**, *75*, 6666−6672.
(29) Zhang, X.-B.; Wang, Z.; Xing, H.; Xiang, Y.; Lu, Y. Catalytic and Molecular Beacons for Amplified Detection of Metal Ions and Organic Molecules with High Sensitivity. *Anal. Chem.* **2010**, *82*, 5005−5011.
(30) Sun, C.; Zhang, L.; Jiang, J.; Shen, G.; Yu, R. Electrochemical DNA Biosensor Based on Proximity-Dependent DNA Ligation Assays with DNAzyme Amplification of Hairpin Substrate Signal. *Biosens. Bioelectron.* **2010**, *25*, 2483−2489.
(31) Diao, W.; Tang, M.; Ding, X.; Zhang, Y.; Yang, J.; Cheng, W.; Mo, F.; Wen, B.; Xu, L.; Yan, Y. Electrochemical DNA Biosensor Based on MNAzyme-Mediated Signal Amplification. *Microchim. Acta* **2016**, *183*, 2563−2569.
(32) Zagorovsky, K.; Chan, W. C. W. A Plasmonic DNAzyme Strategy for Point-of-Care Genetic Detection of Infectious Pathogens. *Angew. Chem., Int. Ed.* **2013**, *52*, 3168−3171.
(33) Chen, Y.; Corn, R. M. DNAzyme Footprinting: Detecting Protein−Aptamer Complexation on Surfaces by Blocking DNAzyme Cleavage Activity. *J. Am. Chem. Soc.* **2013**, *135*, 2072−2075.
(34) Li, X.; Cheng, W.; Li, D.; Wu, J.; Ding, X.; Cheng, Q.; Ding, S. A Novel Surface Plasmon Resonance Biosensor for Enzyme-Free and Highly Sensitive Detection of MicroRNA Based on Multi Component Nucleic Acid Enzyme (MNAzyme)-Mediated Catalyzed Hairpin Assembly. *Biosens. Bioelectron.* **2016**, *80*, 98−104.
(35) Kim, J. H.; Han, S. H.; Chung, B. H. Improving Pb2+ Detection Using DNAzyme-Based Fluorescence Sensors by Pairing Fluorescence Donors with Gold Nanoparticles. *Biosens. Bioelectron.* **2011**, *26*, 2125−2129.
(36) Chen, J.; Zuehlke, A.; Deng, B.; Peng, H.; Hou, X.; Zhang, H. A Target-Triggered DNAzyme Motor Enabling Homogeneous, Amplified Detection of Proteins. *Anal. Chem.* **2017**, *89*, 12888−12895.
(37) Swearingen, C. B.; Wernette, D. P.; Cropek, D. M.; Lu, Y.; Sweedler, J. V.; Bohn, P. W. Immobilization of a Catalytic DNA Molecular Beacon on Au for Pb(II) Detection. *Anal. Chem.* **2005**, *77*, 442−448.
(38) Teh, H. B.; Li, H.; Li, S. F. Y. Highly Sensitive and Selective Detection of Pb 2+ Ions Using a Novel and Simple DNAzyme-Based Quartz Crystal Microbalance with Dissipation Biosensor. *Analyst* **2014**, *139*, 5170−5175.
(39) Zhang, B.; Liu, B.; Zhou, J.; Tang, J.; Tang, D. Additional Molecular Biological Amplification Strategy for Enhanced Sensitivity of Monitoring Low-Abundance Protein with Dual Nanotags. *ACS Appl. Mater. Interfaces* **2013**, *5*, 4479−4485.
(40) Zhang, X.-B.; Kong, R.-M.; Lu, Y. Metal Ion Sensors Based on DNAzymes and Related DNA Molecules. *Annu. Rev. Anal. Chem.* **2011**, *4*, 105−128.
(41) Homola, J. Surface Plasmon Resonance Sensors for Detection of Chemical and Biological Species. *Chem. Rev.* **2008**, *108*, 462−493.

DOI: 10.1021/acsami.8b18756
ACS Appl. Mater. Interfaces 2019, 11, 6759−6768

(42) Nguyen, H.; Park, J.; Kang, S.; Kim, M. Surface Plasmon Resonance: A Versatile Technique for Biosensor Applications. *Sensors* **2015**, *15*, 10481−10510.
(43) Caucheteur, C.; Guo, T.; Albert, J. Review of Plasmonic Fiber Optic Biochemical Sensors: Improving the Limit of Detection. *Anal. Bioanal. Chem.* **2015**, *407*, 3883−3897.
(44) Gupta, B. D.; Kant, R. [INVITED] Recent Advances in Surface Plasmon Resonance Based Fiber Optic Chemical and Biosensors Utilizing Bulk and Nanostructures. *Opt. Laser Technol.* **2018**, *101*, 144−161.
(45) Pollet, J.; Delport, F.; Janssen, K. P. F.; Jans, K.; Maes, G.; Pfeiffer, H.; Wevers, M.; Lammertyn, J. Fiber Optic SPR Biosensing of DNA Hybridization and DNA−protein Interactions. *Biosens. Bioelectron.* **2009**, *25*, 864−869.
(46) Bedford, E. E.; Spadavecchia, J.; Pradier, C.-M.; Gu, F. X. Surface Plasmon Resonance Biosensors Incorporating Gold Nanoparticles. *Macromol. Biosci.* **2012**, *12*, 724−739.
(47) Knez, K.; Janssen, K. P. F.; Pollet, J.; Spasic, D.; Lammertyn, J. Fiber-Optic High-Resolution Genetic Screening Using Gold-Labeled Gene Probes. *Small* **2012**, *8*, 868−872.
(48) Daems, D.; Peeters, B.; Delport, F.; Remans, T.; Lammertyn, J.; Spasic, D. Identification and Quantification of Celery Allergens Using Fiber Optic Surface Plasmon Resonance PCR. *Sensors* **2017**, *17*, 1754.
(49) Lu, J.; Van Stappen, T.; Spasic, D.; Delport, F.; Vermeire, S.; Gils, A.; Lammertyn, J. Fiber Optic-SPR Platform for Fast and Sensitive Infliximab Detection in Serum of Inflammatory Bowel Disease Patients. *Biosens. Bioelectron.* **2016**, *79*, 173−179.
(50) Daems, D.; Lu, J.; Delport, F.; Mariën, N.; Orbie, L.; Aernouts, B.; Adriaens, I.; Huybrechts, T.; Saeys, W.; Spasic, D.; et al. Competitive Inhibition Assay for the Detection of Progesterone in Dairy Milk Using a Fiber Optic SPR Biosensor. *Anal. Chim. Acta* **2017**, *950*, 1−6.
(51) Todd, A. V.; Fuery, C. J.; Impey, H. L.; Applegate, T. L.; Haughton, M. A. DzyNA-PCR: Use of DNAzymes to Detect and Quantify Nucleic Acid Sequences in a Real-Time Fluorescent Format. *Clin. Chem.* **2000**, *46*, 625−630.
(52) Chen, J.; Pan, J.; Chen, S. A Naked-Eye Colorimetric Sensor for Hg 2+ Monitoring with Cascade Signal Amplification Based on Target-Induced Conjunction of Split DNAzyme Fragments. *Chem. Commun.* **2017**, *53*, 10224−10227.
(53) Hurst, S. J.; Lytton-Jean, A. K. R.; Mirkin, C. A. Maximizing DNA Loading on a Range of Gold Nanoparticle Sizes. *Anal. Chem.* **2006**, *78*, 8313−8318.
(54) Rasband, W. S. *ImageJ*; U.S. National Institutes of Health: Bethesda, Maryland.
(55) European Medicines Agency: CPMP/ICH/381/95 - ICH Topic Q2 (R1) Validation of Analytical Procedures: Text and Methodology Step 5 Note for Guidance on Validation of Analytical Procedures: Text and Methodology, 1995; July 2018.
(56) Lyon, L. A.; Musick, M. D.; Natan, M. J. Colloidal Au-Enhanced Surface Plasmon Resonance Immunosensing. *Anal. Chem.* **1998**, *70*, 5177−5183.
(57) Knez, K.; Spasic, D.; Delport, F.; Lammertyn, J. Real-Time Ligation Chain Reaction for DNA Quantification and Identification on the FO-SPR. *Biosens. Bioelectron.* **2015**, *67*, 394−399.
(58) Malinský, P.; Slepička, P.; Hnatowicz, V.; Švorčík, V. Early Stages of Growth of Gold Layers Sputter Deposited on Glass and Silicon Substrates. *Nanoscale Res. Lett.* **2012**, *7*, 241.
(59) Markham, N. R.; Zuker, M. DINAMelt Web Server for Nucleic Acid Melting Prediction. *Nucleic Acids Res.* **2005**, *33*, W577−W581.
(60) Markham, N. R.; Zuker, M. UNAFold. In *Bioinformatics, Volume II. Structure, Function and Applications, number 453 in Methods in Molecular Biology*; Keith, J. M., Ed.; Humana Press: Totowa, NJ, 2008; pp 3−31.
(61) Yurke, B.; Turberfield, A. J.; Mills, A. P.; Simmel, F. C.; Neumann, J. L. A DNA-Fuelled Molecular Machine Made of DNA. *Nature* **2000**, *406*, 605−608.
(62) Knez, K.; Janssen, K. P. F.; Spasic, D.; Declerck, P.; Vanysacker, L.; Denis, C.; Tran, D. T.; Lammertyn, J. Spherical Nucleic Acid Enhanced FO-SPR DNA Melting for Detection of Mutations in Legionella Pneumophila. *Anal. Chem.* **2013**, *85*, 1734−1742.
(63) Wei, L.; Wang, X.; Wu, D.; Li, C.; Yin, Y.; Li, G. Proximity Ligation-Induced Assembly of DNAzymes for Simple and Cost-Effective Colourimetric Detection of Proteins with High Sensitivity. *Chem. Commun.* **2016**, *52*, 5633−5636.

DOI: 10.1021/acsami.8b18756
ACS Appl. Mater. Interfaces 2019, 11, 6759−6768